PHYSICAL PROPERTIES OF JETS IN LOW-LUMINOSITY RADIO SOURCES

G. V. BICKNELL,[1] H. R. DE RUITER,[2] R. FANTI,[2,3] R. MORGANTI,[2,4] AND P. PARMA[2]

ABSTRACT

We present the results of fitting Bicknell's semiempirical turbulent jet model to a sample of 23 jets taken from the B2 extragalactic radio sources studied in detail using the VLA (Fanti et al.). We find that the model fits are generally very reasonable (especially for the smoother jets) and that the single most important parameter in the fits is the ratio of galaxy virial temperature to interstellar medium temperature. We find a distribution for this parameter which is consistent with the distribution found by Thomas et al. for an independent sample of X-ray–emitting ellipticals. The core radii (~ 1 kpc) inferred from the fits are typical of those found for cD galaxies. In most cases, where we have two jets within the same galaxy the inferred galaxy atmosphere parameters are almost identical. All jets are initially light with respect to the interstellar medium (ISM) and eventually approach density equilibrium through entrainment. The Mach numbers for most jets are in the range from 1 to 3. However, we can identify a high–Mach number subsample for which the Mach numbers could be as high as 10. Significantly these jets are lighter, better collimated, and more powerful than the rest of the sample, supporting the notion that the transition from class I to class II radio sources represents in large part, a transition from low– to high–Mach number jets. The velocities of all the jets in the sample range between ~ 1000–10,000 km s^{-1} with the high–Mach number subsample having velocities at the upper end of this range. The jet velocities are consistent with the energy budget in each source (except one), with the qualification that the velocities of some low-velocity jets may be underestimated. It is also possible that these particular sources are approximately in radiative equilibrium. We estimate the mass-to-light ratios for the parent galaxies and find a mean value (for $H_0 = 100$) of 24 ± 5, somewhat higher than the usual core mass-to-light value of 14. However, these values need to be reassessed in the light of higher quality photometric and spectroscopic data.

Subject headings: galaxies: jets — radio sources: galaxies

I. INTRODUCTION

Large kpc–scale radio jets are frequently detected in low-luminosity radio sources (class I sources in the terminology of Fanaroff and Riley 1974): as many as one-half of all radio sources with $P_{1.4 \, \text{GHz}} < 10^{24.5}$ W Hz^{-1} have well-defined and recognizable jets. Moreover, class I sources tend to be symmetric, with jets of comparable strength on both sides.

Unlike the jets in the high-powered class II sources, class I jets appear to be only mildly supersonic, so that numerical models developed for the former type of jets (Norman, Winkler, and Smarr 1984) do not apply. In particular, entrainment of external material is fundamental, for a correct description of jets in low-luminosity sources. The correct estimation of the amount of entrainment and the related deceleration is necessary for the calculation of the variation of surface brightness along the length of the jet. This was emphasized by Bicknell (1984), who, in a series of papers, developed a model for turbulent, low–Mach number jets (Bicknell 1984, 1986a, b, hereafter B84, B86a, and B86b, respectively). He applied this model to a few well-studied objects, but it remained to be seen if the picture given by him is satisfactory in general for a large number of low-luminosity sources. This is important, not only for verification of the general physical ideas involved in these

models, but also for the estimation of jet velocities. Given that one can estimate (at least to within factors of order unity) the critical jet parameters, density ratio, and Mach number, we have a way of estimating the jet velocity also to within a factor of order unity, provided we know the temperature of the galaxy atmosphere. Alternatively, if the low–Mach number approximation for class I jets proves to be correct, then consideration of the energy budget (B86a) gives a direct way of calculating the velocity.

Another idea which arises from the cited papers is that the division between Fanaroff-Riley class I and class II sources reflects, to a large extent, a difference in the Mach numbers of their respective jets.

Therefore, the main purpose of this paper is to test the low–Mach number turbulent jet model of B86b and its main physical ideas, using a much larger data base, and to use this model in a systematic study of the parameters of jets in low-luminosity sources. In particular, we investigate whether the proposed jet model is consistent with the parameters of galaxy atmospheres as determined from the sample of X-ray–emitting ellipticals studied by Thomas et al. (1986). We also examine fits to the data for their internal consistency; for example, we examine closely the behavior of density ratio, velocity, and surface brightness in the collimation plateaus of the jets in the sample.

This paper is organized as follows. In § II, we summarize the radio data and describe the sample of radio sources used in this study. In § III, we discuss the procedure for fitting the model to the data; the results are discussed in § IV. Our conclusions are presented in § V.

[1] Mount Stromlo and Siding Spring Observatories, Institute of Advanced Studies, Australian National University.
[2] Istituto di Radio Astronomia del CNR, Bologna, Italy.
[3] Dipartimento di Astronomia, Università di Bologna, Bologna, Italy.
[4] European Southern Observatory, Garching, Federal Republic of Germany.

II. THE RADIO DATA

Recently, a study was carried out with the VLA of a complete sample of low-luminosity radio galaxies selected from the B2 Catalog. This sample consists of ~100 objects, most of which have been observed at 1.4 GHz with the VLA in three different configurations (resolution ranging from ~1".3 to ~13"). The observations, together with the radio maps and a discussion of the data reduction, were presented in four separate papers (Parma *et al.* 1986; de Ruiter *et al.* 1986; Fanti *et al.* 1986; Fanti *et al.* 1987; Papers I–IV, respectively). We refer to these papers for details on the definition of the sample.

A polarization study of five sources selected from this sample is given in Morganti *et al.* (1987, Paper V).

Since the majority of the sources have a power $P_{1.4} < 10^{25}$ W Hz^{-1}, jets were detected in large numbers; about 45% of the sources show unambiguous evidence for either single or double jets. Therefore, a statistical study of jet properties became feasible; the results of this study can be found in Parma *et al.* (1987, Paper VI).

One of the most important jet quantities is the spreading rate $d\Phi/d\Theta$, the rate of change of jet angular FWHM (Φ) with respect to angular distance from the core (Θ). For every jet, the spreading rate was measured at various distances from the core, and while for about half the jets the data are consistent with a constant spreading rate, in the remainder they are clearly nonconstant. In general, the trend is a phase of expansion followed by a recollimation regime and a further expansion. In phases of expansion, the surface brightness decreases more slowly than in more collimated regions of the jet. This "sub-adiabatic" behavior was the principal reason why nonconstant jet velocities were introduced in the discussion of jet dynamics (Fanti *et al.* 1982).

In order to analyze the jet behavior in terms of the model of B86b, we have selected the best defined jets among those with multiple spreading rate regimes. These are listed in Table 1, where we give the name of the radio source in column (1), the redshift in column (2), the total power at 1.4 GHz in column (3), the absolute visual magnitude of the parent galaxy in column (4), and a jet classification based on the behavior of the brightness in column (5): S ("smooth"), B ("blobby"), or SB (in part smooth and in part blobby) (see Paper VI for more details; note that in the following, the SB jets are considered B).

In Figure 1, the $\Phi - \Theta$ data for all jets listed in Table 1 are shown. The solid curve is a spline fit to the data, which is used as input to the theoretical models.

III. MODEL FITTING

a) Preliminary Remarks

In this section, we describe the procedure used and the results obtained by fitting the turbulent jet model of B86b to the data described in the earlier sections. First, however, we summarize the approach inherent in this model. The model is a semiempirical one in which the observed spreading rate is used to infer the change of velocity and surface brightness through equations describing the conservation of mass, momentum, and energy and another equation describing the phase-space evolution of the relativistic electron distribution. An approximation used is that the jet flow is adiabatic, and this is reasonable for transonic flow or for higher Mach number jets, in which the spreading induced by turbulence is not great. This adiabatic assumption is likely to be less accurate when there is evidence of dissipation in the form of bright "blobs" or other

TABLE 1

THE SAMPLE OF CLASS I JETS

Source (1)	Redshift (2)	log P (3)	M_v (4)	Jet Classification (5)
0034+25	0.0321	23.13	−21.3	...
East jet	...	22.30	...	S
West jet	...	22.30	...	S
0206+35	0.0375	24.50	−21.8	...
East jet	...	23.32	...	S
West jet	...	23.46	...	S
0755+35	0.0413	24.49	−21.8	...
East jet	...	23.52	...	S
0836+29	0.0790	24.73	−22.4	...
North jet	...	23.85	...	B
1113+29	0.0489	24.67	−21.8	...
West jet	...	23.34	...	B
1243+26	0.0891	24.22	−22.1	...
North jet	...	23.97	...	SB
South jet	...	23.12	...	SB
1357+28	0.0629	24.03	−21.9	...
North jet	...	23.44	...	SB
South jet	...	23.00	...	B?
1450+28	0.1265	24.33	−21.6	...
East jet	...	23.81	...	SB
West jet	...	21.89	...	B?
1521+28	0.0825	24.58	−21.7	...
South jet	...	23.80	...	SB
1553+24	0.0426	23.36	−21.2	...
East jet	...	22.69	...	S
West jet	...	22.93	...	S
1638+32	0.1398	24.80	−22.6	...
West jet	...	24.06	...	B?
1658+30	0.0351	23.88	−20.6	...
West jet	...	23.17	...	S?
1752+32	0.0449	23.47	−21.6	...
East jet	...	28.87	...	?
West jet	...	23.13	...	S
1827+32	0.0659	24.07	−21.9	...
East jet	...	22.80	...	S
West jet	...	22.90	...	SB
2116+26	0.0164	22.48	−21.1	...
South jet	...	21.89	...	SB

rapid localized variations in surface brightness. This is borne out in the model fits, which are better, in general, for the smoother jets (see § IV).

Previous fits to the surface brightness of 3C 31 and NGC 315 (B84 and B86b) suggest that the following factors are important in the propagation of class I jets. Initially, jet turbulence is responsible for the initial spreading rate. Sometimes the level of turbulence appears to decrease, possibly because of a transition to nonturbulent flow mediated by a "favorable" pressure gradient. When this occurs, the jet recollimates. If the jet is still buoyant at this stage, it accelerates, and its surface brightness decreases more rapidly. This situation persists until the jet meets a less favorable pressure gradient as it ploughs into the approximately constant pressure of the surrounding intergalactic medium (IGM). A reexpansion of the jet ensues, accompanied by a slower decrease in surface brightness. The data used in this paper are a very useful set for the examination of these ideas, because many of the jets exhibit three different regimes of collimation.
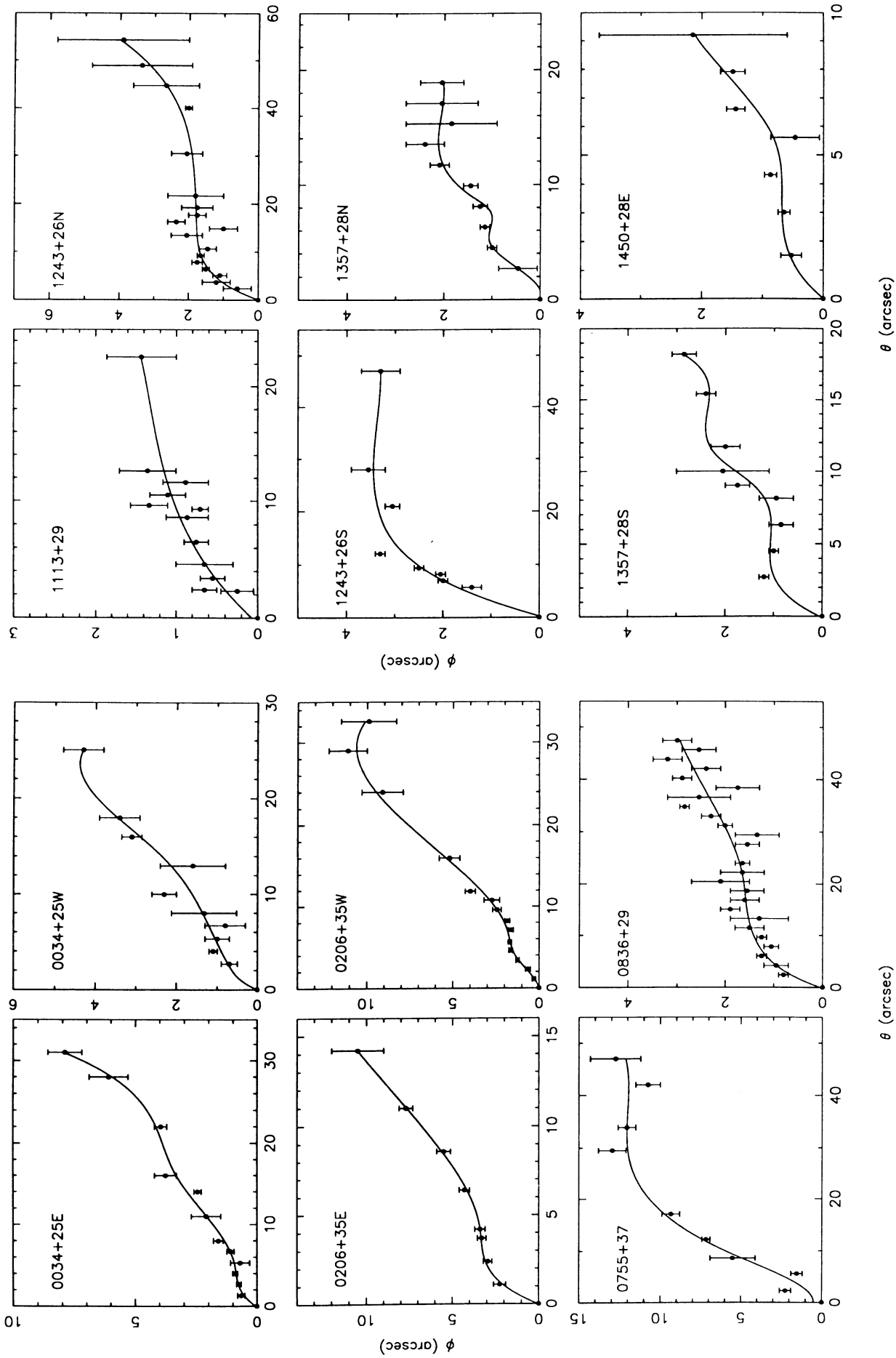
FIG. 1.—FWHM jet diameter Φ against distance Θ from the radio core. The solid line is a spline fit to the data.
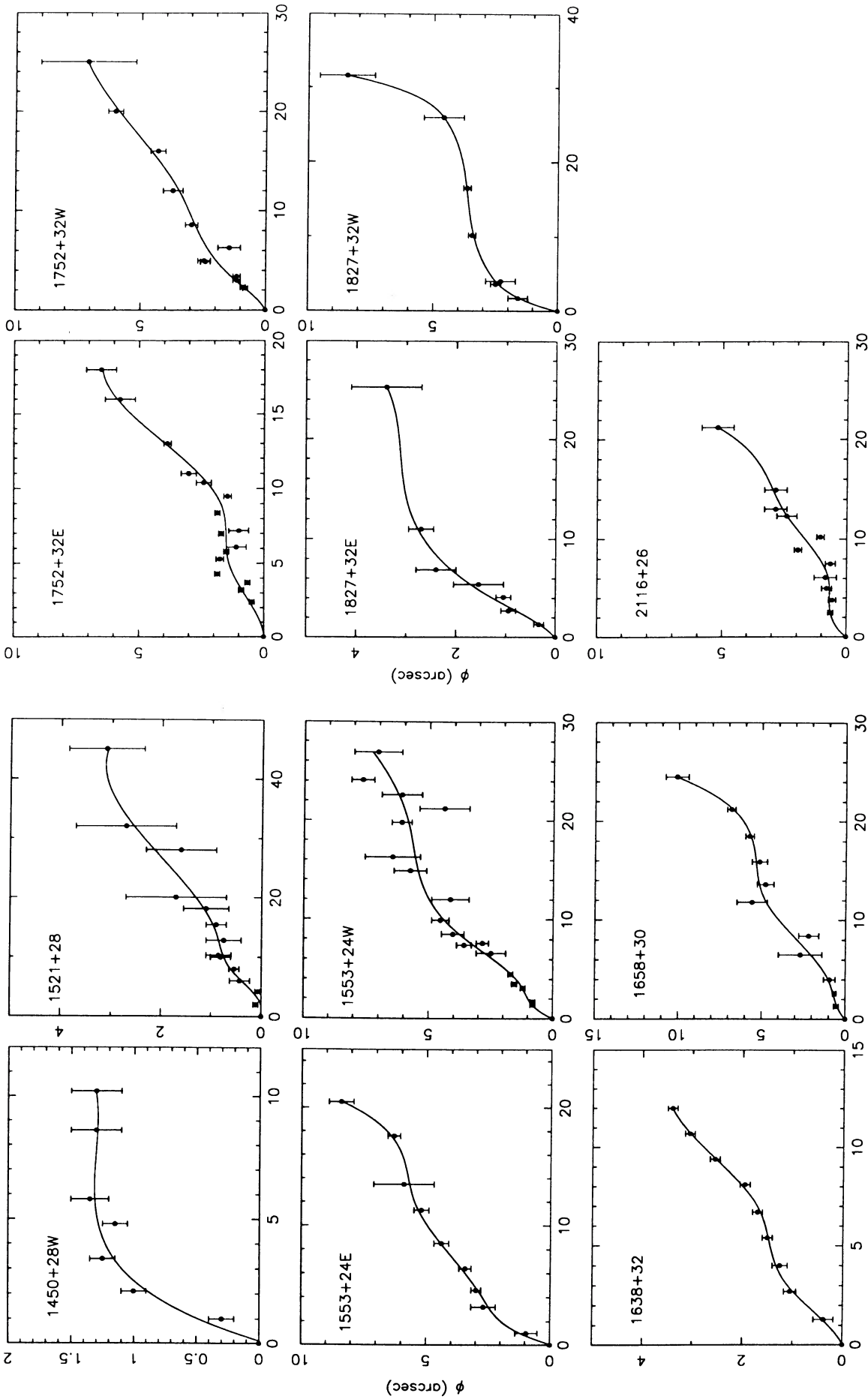
FIG. 1—Continued

101

The following parameters enter into the semiempirical model. The most important parameter is β, the ratio of the virial temperature of the galaxy to the temperature of the interstellar medium. This parameter determines the rate of change of the pressure with distance from the center of the galaxy and governs, through pressure equilibrium, the internal energy density of the jet as a function of distance from the core. It also determines the buoyancy force, and this is extremely important when the jet surface brightness drops rapidly along a collimation plateau. The next most important parameter is η, the ratio of jet density to ISM density at a specified fiducial point along the jet. The lower the value of η, the more rapidly the jet is decelerated by entrainment but the greater the buoyancy force acting upon it. The initial jet Mach number also influences the inferred variation of velocity. However, the influence of this parameter is not nearly as great as that of the previous two; in most cases, the best fits are obtained with the Mach number between 1 and 3.

In order for a physically consistent pressure profile to be used, it is necessary that one adopt a physically consistent form for the galactic potential. We use a $W_0 = 9.5$ King potential (typically used in fits to the surface brightness of elliptical galaxies), whose core radius r_c is a free parameter. Effectively, the parameter which is varied is $r_{c,p} = r_c \sin i$ (i = inclination of jet to line of sight), the core radius projected along the jet. Since the jets we have selected are well defined in general, it is likely that in most cases $\sin i \approx 1$. The main effect of the core radius is that it determines the distance from the center of the galaxy at which the pressure profile flattens and hence the point at which a *light* jet should start to reexpand. The following expression for the pressure $P(r)$ of an isothermal atmosphere illustrates this point:

$$\frac{P(r)}{P_c} = \exp\left(-\beta\frac{\phi}{\sigma_p^2}\right), \tag{3.1}$$

where P_c is the central pressure, $\beta = T_*/T$ is the ratio of the virial temperature to the atmospheric temperature, ϕ is the gravitational potential with respect to the center of the galaxy, and σ_p is the central projected velocity dispersion. This pressure asymptotically approaches a background value given by

$$\frac{P_\infty}{P_c} = \exp\left(-\beta\frac{\phi_\infty}{\sigma_p^2}\right), \tag{3.2}$$

where ϕ_∞ is the total depth of the potential well. The core radius provides a scale for the radius and determines how quickly the potential approaches its background value and hence how quickly the pressure flattens out. Thus the core radius, as it enters the models used here, relates primarily to the behavior of the potential of the outer parts of the galaxy, and a large fitted value may, in fact, compensate for the depth of the potential well described by the King model. Thus, the parameter r_c may not accurately represent the optically measured core radius of the galaxy. For instance, if the galaxy has a power-law surface brightness profile, then, for a given core radius, its potential well will be deeper than that of a $W_0 = 9.5$ King potential. Another way in which the inferred core radius could be unphysically increased is if the temperature of the atmosphere decreases at large radii. The relevant background pressure would then be lower, and the radius at which the pressure flattens to the background would be higher. Within the present constraint of an isothermal atmosphere, the only way in which this can be mimicked is for the core radius to

increase. On the other hand, a higher value of the core radius than would be reasonable for the optical galaxy could also be indicative of an underlying dark matter distribution. Thus, it will be of interest to compare the core radii inferred from these models with values obtained from future optical and X-ray data.

b) Minimum Pressure Fits

In view of the number of independent parameters used in the semiempirical model in our first attempt at obtaining model fits, we restricted the relevant values of β and the projected core radius $r_c \sin i$, using the minimum pressure of the jets. We evaluated the minimum pressure at independent points (separated by a beam size) along the length of each jet and fitted, by eye, the atmosphere described by equation (3.1). The rationale behind this procedure is that, while the surface brightness and jet radius do not uniquely define the jet pressure, the minimum value is not a sensitive function of the ratio of particle pressure to magnetic pressure when the former dominates the latter. (The total pressure changes by approximately a factor of 2 when the ratio of particle pressure to magnetic pressure increases by a factor of 10 from the minimum pressure value.) Since the complementary regime in which the magnetic pressure dominates the particle pressure is likely to be unstable, it is quite probable that the minimum pressure traces the shape, if not the absolute value, of the pressure profile of the confining atmosphere. The model fits to the minimum pressure are shown in Figure 2, and the values of the parameters r_c and β are recorded in Table 2 (r_c in cols. [4] and [5] and β in col. [6]). The starred pressure values in Figure 2 are the minimum pressures calculated for the lobes.

The projected core radii are plotted against redshift in Figure 3, and there is no correlation between these two variables, indicating that no systematic bias has been introduced into the fitting procedure. Some of the core radii are reasonably large (of the order of 1–2 kpc; see § IVa), and it is possible that some, if not all, of these galaxies are cD's, in which case optical core radii of this magnitude are quite reasonable. Other reasons for a large inferred core radius have also been discussed above. Optical studies, both in progress and planned, of these galaxies should provide further useful information.

For most of the galaxies, the core radii are constrained mainly by the jet minimum pressures in the outer parts of the galaxy. However, in two cases, B2 0034+25 and B2 2116+26, the fits are strongly influenced by the values of the minimum pressure close to the nucleus. For the former galaxy, $r_c = 1.9$ kpc and for the latter $r_c \approx 1.2$ kpc. Detailed surface photometry of these galaxies (but in particular B2 0034+25) would therefore be of interest.

c) Model Fits to the Surface Brightness

The fundamental input to the semiempirical model is the jet FWHM data. A spline fit to these data (Fig. 1) is used to define the variation of FWHM (Φ) as a function of angular distance from the core (Θ).

We have used two approaches to fit models to the surface brightness. In the first approach, the values of β and $r_c \sin i$ were fixed at the values derived from the minimum pressure fits, and we varied the parameters η_0, the density ratio of the jet at an assigned fiducial point Θ_0 (see col. [3] of Table 2), and $\mathcal{M}_0$, the Mach number at that point, together with a parameter for scaling the surface brightness ($I_{v,0}$). Another parameter which can be important is $B_\parallel/B_p$, the ratio of longitudinal to
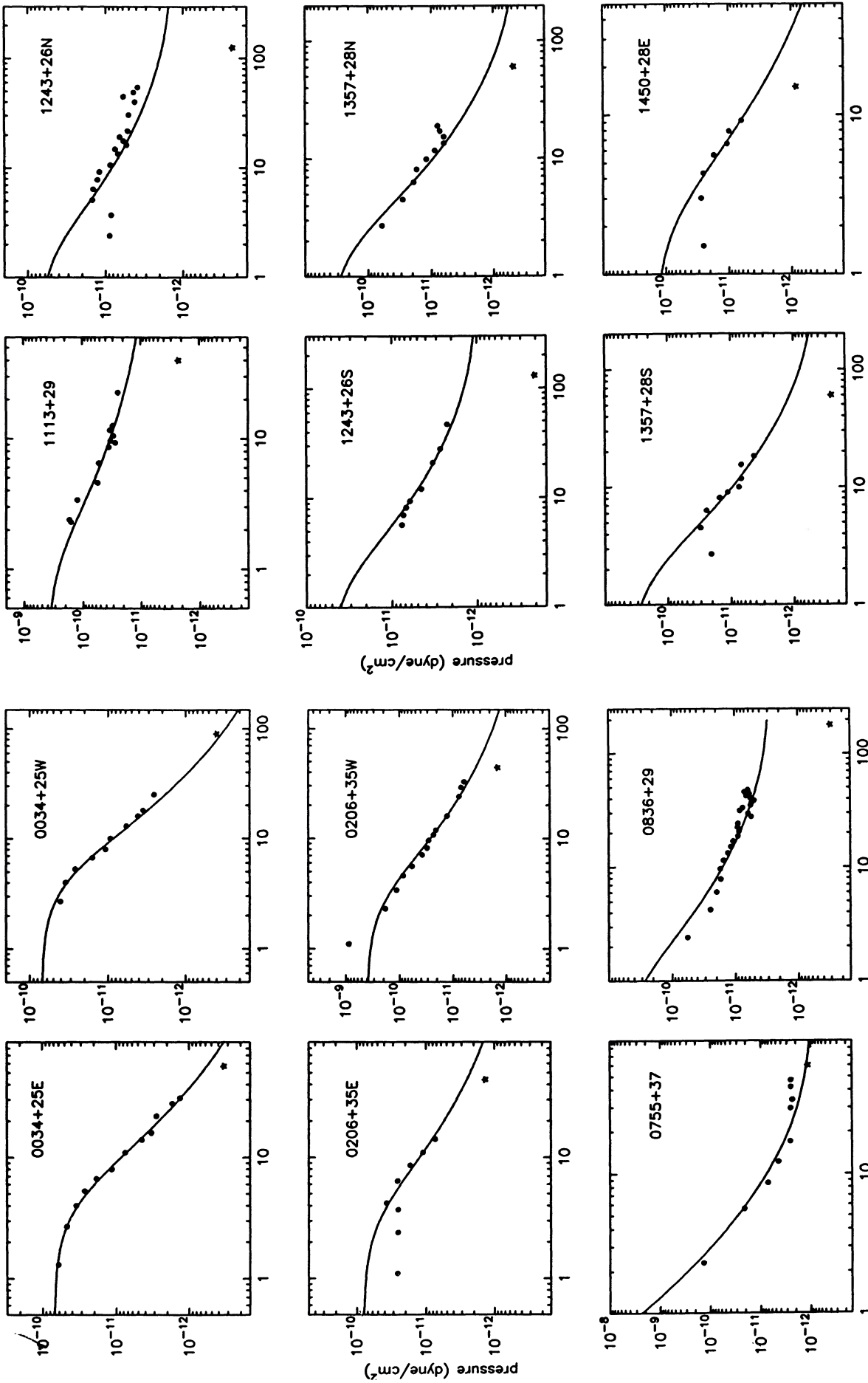
Fig. 2.—The minimum pressure of the jet measured at various distances from the core (*dots*). The asterisk represents the minimum pressure of the radio lobe. The solid line, a King model of the galactic atmosphere (see text), is a best fit to the slope of the jet minimum pressure.
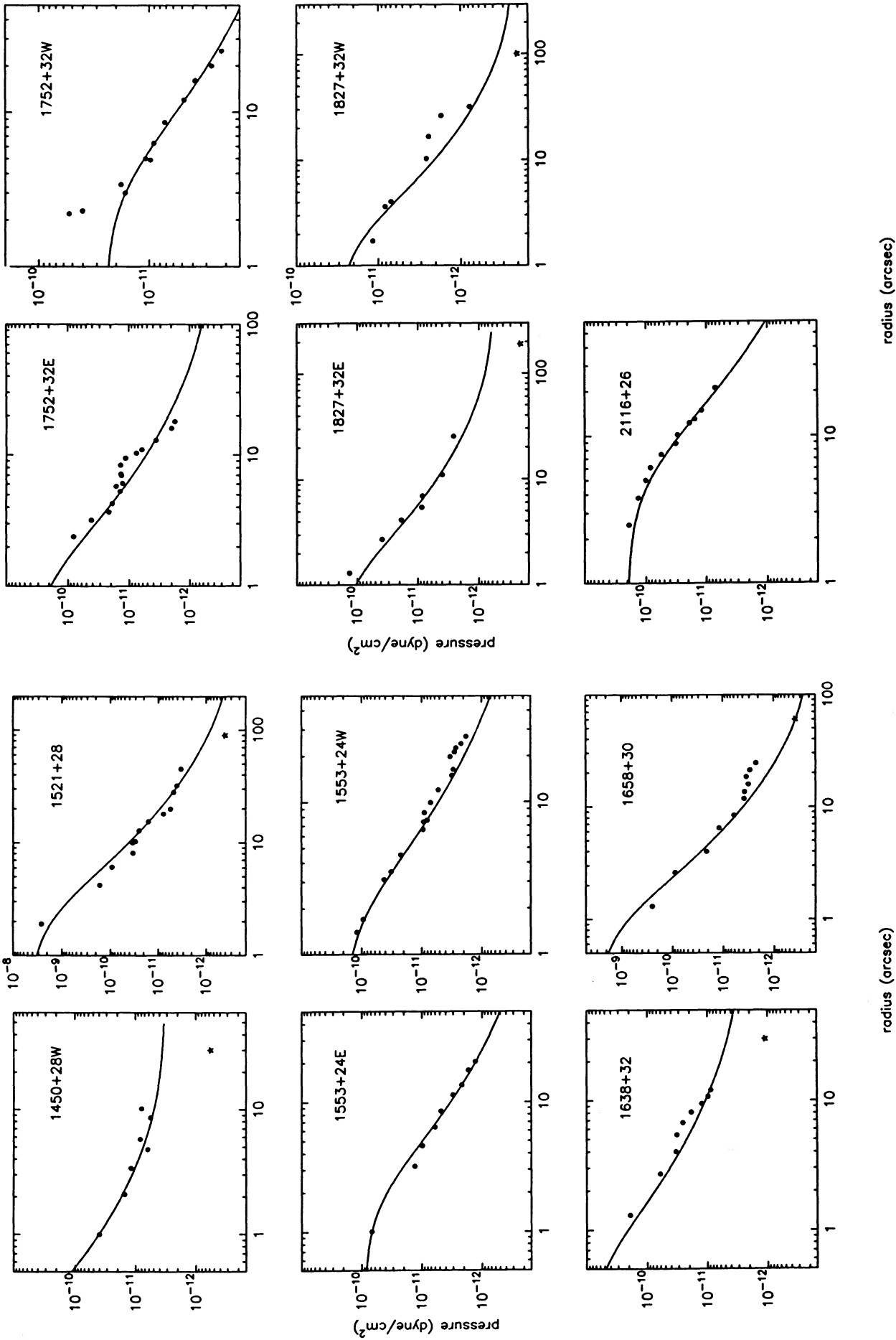
103

Fig. 2—Continued

radius (arcsec)

pressure (dyne/cm²)

104

TABLE 2

BEST-FIT VALUES OF PARAMETERS

JET (1)	$B_\|/B_p$ (2)	Θ_0 (3)	FIXED BY MINIMUM PRESSURE						FREE FITS			
			$r_{c,p}$ (4)	$r_{c,p}$ (kpc) (5)	β (6)	η_0 (7)	$\mathcal{M}_0$ (8)	χ_r^2 (9)	$r_{c,p}$ (10)	β (11)	η_0 (12)	$\mathcal{M}_0$ (13)
0034E	0	2".7	4".0	1.8	0.70	0.78	1.9	1.20	4".0	0.70	0.78	1.9
0034W	0	4.0	4.0	1.8	0.70	0.09	1.0	1.24	4.0	0.70	0.09	1.0
0206E	0	4.2	3.0	1.6	0.50	0.50	3.5	...	4.0	0.50	0.63	3.5
0206W	1	2.3	2.5	1.3	0.65	0.03	2.0	1.18	2.5	0.65	0.03	2.0
0755E	0	5.6	0.3	0.2	1.30	0.66	1.4	2.12	0.3	1.30	0.66	1.4
0836N	0	9.6	0.8	0.8	0.55	0.10	1.6	4.55	0.8	0.55	0.10	1.6
1113W	1	4.6	1.0	0.7	0.40	0.06	4.0	4.22	0.5	0.30	0.50	4.0
1243N	0	9.2	1.5	1.7	0.40	0.02	2.0	5.06	1.0	0.40	0.06	2.0
1243S	0	7.0	1.5	1.7	0.40	0.25	3.0	2.85	1.0	0.40	0.25	1.5
1357N	0	4.5	1.5	1.3	0.70	1.00	1.5	7.77	4.0	0.50	0.40	1.3
1357S	0	4.5	1.5	1.3	0.70	0.79	1.0	7.38	1.5	0.70	0.79	1.0
1450E	0	3.0	2.0	3.0	0.70	1.00	1.0	6.20	2.0	0.70	1.00	1.0
1450W	0	2.1	0.1	0.2	0.70	1.00	2.0	9.67	0.1	0.70	1.00	2.0
1521S	1	4.2	2.0	2.1	1.00	0.01	3.0	13.2	2.0	1.00	0.01	3.0
1553E	0	3.2	1.7	1.0	0.65	1.00	3.0	7.96	1.7	0.65	1.00	3.0
1553W	0	1.7	1.6	0.9	0.70	0.08	1.5	5.84	1.6	0.70	0.08	1.5
1638W	0	2.7	0.5	0.8	0.60	1.00	2.0	9.26	0.5	0.60	1.00	2.0
1658W	0	2.6	0.8	0.4	1.00	0.66	1.8	18.3	1.0	0.80	0.40	1.0
1752E	1	3.7	1.0	0.6	0.70	0.20	3.0	19.3	0.5	0.70	0.79	3.0
1752W	1	3.0	3.0	1.8	0.40	0.10	2.5	2.97	3.0	0.40	0.10	2.5
1827E	0	2.7	1.0	0.9	0.60	0.40	1.0	2.12	1.0	0.60	0.40	1.0
1827W	0	3.6	1.5	1.3	0.50	0.89	1.5	9.00	1.5	0.50	0.89	1.5
2116S	0	3.8	5.0	1.2	0.80	0.63	1.3	1.99	5.0	0.80	0.63	1.3

perpendicular field at the fiducial point. However, class I jets are normally only parallel field–dominated close to the core (Bridle 1984), and the redshift of these sources is on average large enough that, in most cases, the assumption $B_\|/B_p = 0$ is sufficient. For some nearby sources for which polarization data are available, we have information on the field transition point, and where this is the case we have taken $B_\|/B_p = 1$ there (see Table 2, col. [2]). A grid of models was calculated in which the above three parameters were varied and the best-fit model was determined from the minimum χ^2 fit to the surface brightness. The best-fit models are shown as the solid curve in Figure 4, and the corresponding parameters are listed in Table 2.
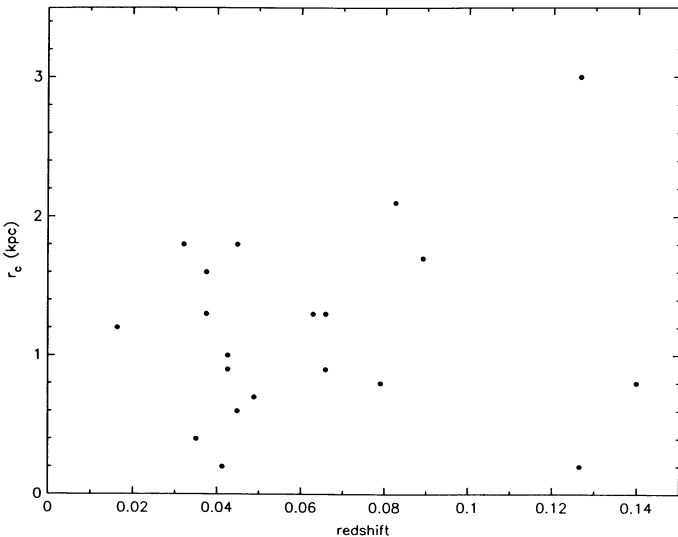

FIG. 3.—The core radii (in kpc), obtained by the minimum pressure fits shown in Fig. 2 against redshift.

Our second approach was to allow all the above parameters (β, η, $r_c \sin i$, $\mathcal{M}$, and $I_{v,0}$) to vary independently. The resulting parameters are also recorded in Table 2, and the model fits are shown as the dashed curve in Figure 4 (but only if they are different from the best fit according to our first method). As can be seen from Table 2, the values of r_c and β that were obtained by the two different methods agree very well in 75% of all cases. In all these fits, the range of parameters was taken to be sufficiently large that the optimum value of χ^2 was found in the interior of the parameter space—not on the boundary. For some choices of parameters, the jet velocity became negative before the end of the jet, and such parameters were naturally discarded. However, it is interesting that the best fits were often obtained for parameter values just inside the region defined by the critical ones. This suggests that in these cases, the optimum parameters are such that the jet has stopped almost completely by the end, and this is consistent with the physical idea that *the extent of these sources is governed by entrainment.*

For most sources, the parameters determined by the two methods agree very well, and there are only four jets out of 23 for which there is some disagreement. However, in only a few cases are the values of χ^2 close to the expected value of v, the number of degrees of freedom. This is due principally to the nature of the ensemble-averaged jet model. In the spline fits to the FWHM, a fit is used which smooths out the excursions to the FWHM from the general trend. This is reflected in a smooth model surface brightness which cannot reproduce the variations in surface brightness associated with the variations in FWHM, which may be due to localized eddies or to shocks. Nevertheless, as an inspection of Figure 4 shows, the minimum χ^2 models reproduce the average surface brightness quite well. In order to obtain a semiquantitative estimate of the allowable range of each parameter, we determined the values of parameters for which the reduced chi-squared (χ^2/v) is ± 1 removed from its minimum value. The appropriate ranges for the

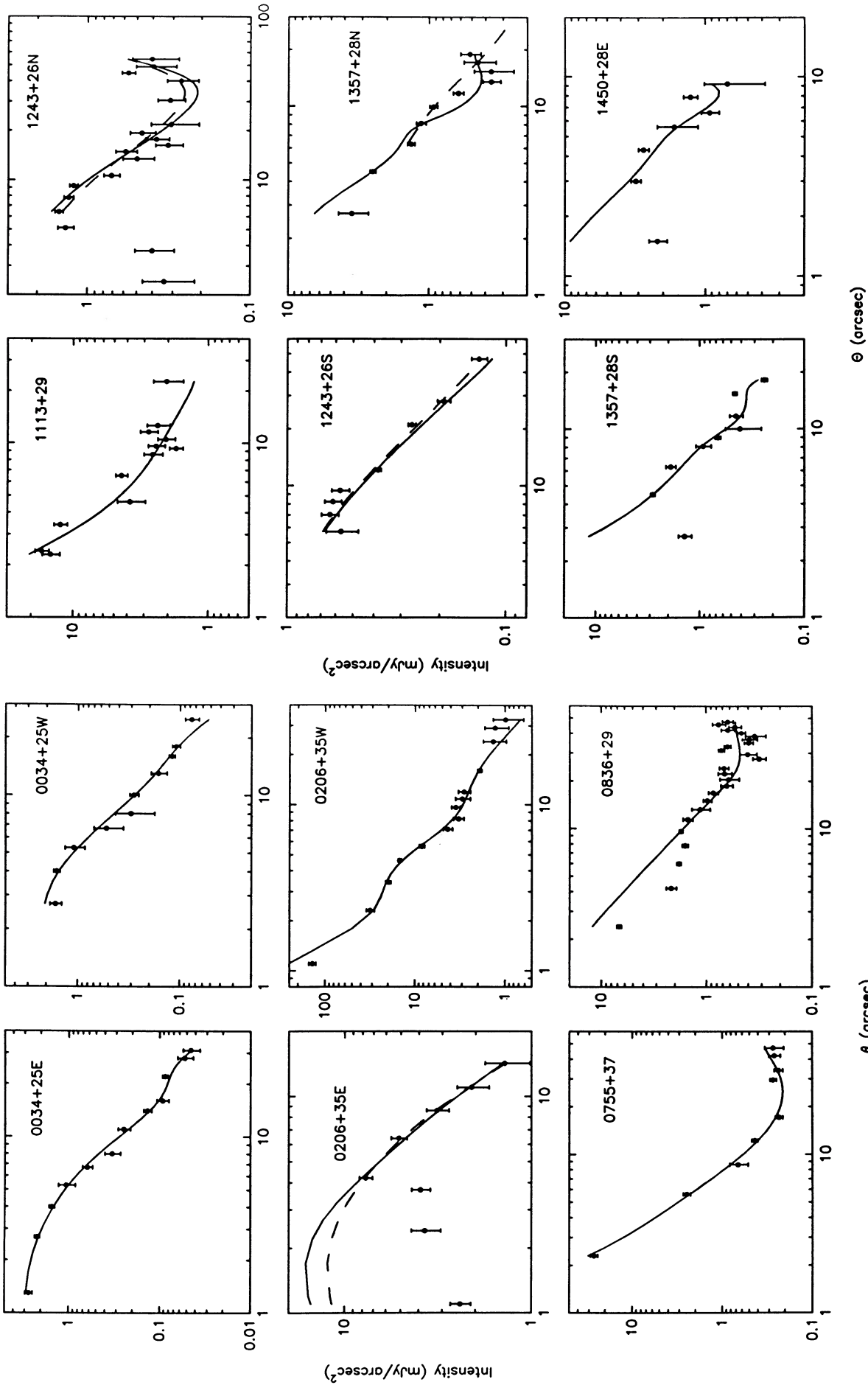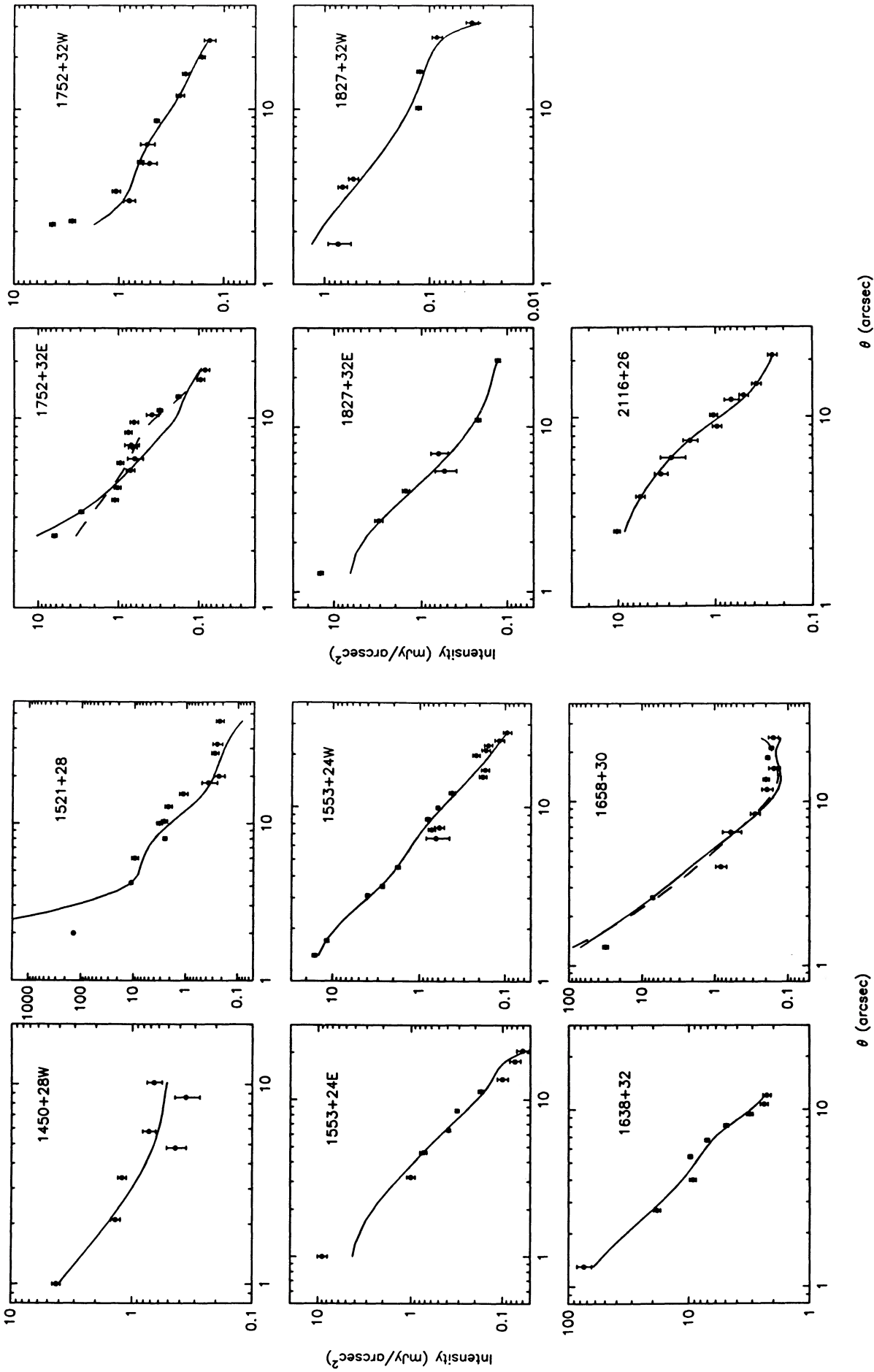FIG. 4.—Brightness model fits. Dots give the brightness (in mJy arcsec^{-2}) measured at various distances from the core. The solid line represents the model with r_c and β fixed by the minimum pressure fit (Fig. 2). If a better "free" fit was found with different values r_c and β, it is shown by a dashed line. Note that the best free fit of B2 1113+29 is practically identical to the model with fixed atmospheric parameters and is therefore not shown separately.

106

FIG. 4—Continued

θ (arcsec)

Intensity (mJy/arcsec²)

1752+32W

1827+32W

1752+32E

1827+32E

2116+26

1521+28

1553+24W

1658+30

1450+28W

1553+24E

1638+32

θ (arcsec)

Intensity (mJy/arcsec²)

107

© American Astronomical Society • Provided by the NASA Astrophysics Data System

TABLE 3

ALLOWABLE RANGE IN FIT PARAMETERS

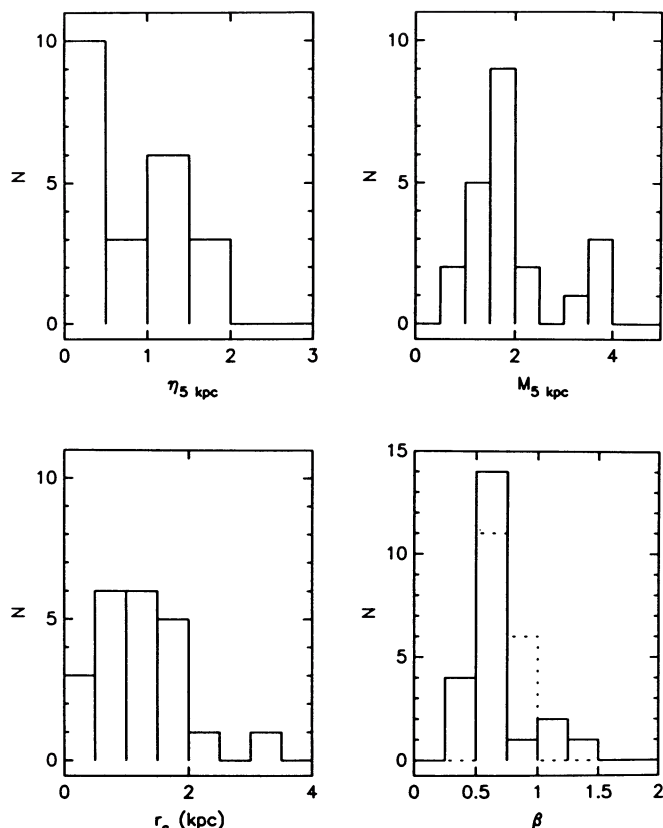| Jet	η_0	β	r_c (arcsec)	$\mathcal{M}_0$
0034E	0.38–0.78	0.60–0.70	...	1.0–2.0
0034W	0.01–0.23	0.70–0.80	...	1.0–3.0
	0.18–0.70	0.60–0.70	...	1.0–1.2
0206W	0.02–0.04	...	...	...
0755E	0.52–0.66	1.00–1.30	0.3–0.6	1.0–1.5
0836N	0.03–032	0.45–0.60	...	1.0–10.0
1113W	0.01–0.20	0.30–0.40	0.5–3.0	1.0–10.0
	0.25–0.80	0.30–0.40	0.5–3.0	1.0–10.0
1243N	0.002–0.16	0.30–0.40	1.0–2.0	1.0–10.0
1243S	0.25–0.51	0.35–0.40	1.0–1.5	1.5–10.0
1357N	0.25–1.00	0.40–0.70	1.0–4.0	1.0–2.0
1450E	0.63–1.00	0.40–0.70	1.0–3.0	1.0–3.5
1450W	0.39–1.00	0.70–0.80	...	1.5–10.0
1521S	0.0001–0.05	...	...	...
1553E	0.81–1.00	...	...	2.5–8.0
1553W	0.04–0.16	0.65–0.70	1.3–1.7	1.5–3.0
1638W	0.94–1.00	...	...	2.0–3.0
1658W	0.40–0.66	0.80–1.00	0.8–1.0	1.0–1.8
1752E	...	...	...	3.0–10.0
1752W	0.015–0.15	...	...	0.8–4.0
1827E	0.40–0.50	0.60–0.70	1.0–2.0	1.0–1.5
1827W	0.79–0.89	0.50–0.55	1.0–1.5	1.5–1.7
2116S	0.25–0.63	0.60–0.80	3.0–5.0	1.0–2.0

FIG. 5.—Histograms of the model parameters. *Upper left panel*: the density ratio η_5 at 5 kpc from the core. *Upper right*: the Mach number at 5 kpc. *Lower left*: the core radius in kpc of the galactic atmosphere. *Lower right*: the solid line gives β as determined from the minimum pressure fits; the dashed histogram gives β as determined from X-ray data of a different sample of objects (Thomas *et al.* 1986).

various values are given in Table 3. From this table, it is evident that for all fits, the most sensitive parameter is β, followed by η and r_c. The least sensitive parameter is the Mach number. Thus, even though each jet is described by a moderate number of parameters, there is a reasonable range in the parameters other than β for which acceptable fits can be obtained. It should be noted that, in one sense, these estimates of the allowable range of the parameters do not adequately convey the region of parameter space for satisfactory model fits. The allowable range of values of η, for instance, depends to some extent upon the Mach number. However, the values quoted are indicative of the region of parameter space involved.

IV. DISCUSSION

a) The Galactic Atmosphere Parameters: r_c and β

The histograms of r_c and β are shown in Figure 5. It can be seen that the core radius is generally close to 1 kpc; in fact, the average value is 1.2 ± 0.7 kpc. According to Hoessel (1980), core radii of giant ellipticals are of the order of 0.2 kpc, whereas cD galaxies typically have $r_c \sim 2$ kpc. Since the B2 galaxies form a mixture of giant ellipticals and cD galaxies, and despite our reservations (expressed in § III) about the relationship of these core radii to optically determined values, the r_c values shown in Figure 5 appear to be quite plausible. As we indicated in § III, it is of interest to compare our model estimates with estimates obtained from optical surface photometry.

As discussed in § III, the parameter r_c mainly determines the region where the external pressure flattens out to the background value, and in galaxies where the core may be resolved by the radio data, it can also constrain the core radius of the underlying matter distribution. For these reasons, r_c can be determined well if the minimum pressure or surface brightness profiles show significantly flat parts either near the nucleus or at the outer ends of the jet. We have a check on the reliability of r_c in cases where we have jets on both sides of the nucleus, because we expect the two sides to have approximately the

same atmospheric parameters, apart from slight distortions due to, e.g., the presence of a companion. For the eight sources with double jets, six gave small differences in r_c as derived from the two sides (see Table 2), and among them are the sources which allowed very satisfactory model fits (B2 0034+25, 0206+35, and 1553+24). The two sources with very different core radii on both sides are B2 1450+28 and 1752+32; it is probably no coincidence that the fits for these sources were less satisfactory, and, moreover, the core radius could not be well constrained, because of the lack of observations both in the inner and in the outer flat part of the pressure profile. Note that for these two sources, the minimum pressure fits on the two sides give very different central pressures (the discrepancy being a factor of 10–20). This clearly unphysical result indicates once again that the model fits for these two sources (at least on one side) are unreliable. However, for the other sources with double jets, the fits give very similar central pressures.

Both the minimum pressure and the model surface brightness fits more tightly constrain the parameter β, because this determines the slope of the galactic atmosphere. This restricts the possible range of values in two independent ways, and, reassuringly, the best model fit usually also gives the value required by the minimum pressure profile. For the entire sample, we find $\bar{\beta} = 0.67 \pm 0.21$; only three jets have $\beta \geq 1.0$. In Figure 5, we show for comparison the histogram of β values derived from X-ray data for a different sample of galaxies (Thomas *et al.* 1986). The mean value of β determined from the

TABLE 4

THE COLLIMATION PLATEAUS

Group (1)	Jet (2)	Region (arcseconds) (3)	Region (kpc) (4)	η (initial–final) (5)	$dP/d\Theta$ (6)	$dv/d\Theta$ (7)	η_5 (8)	$\mathcal{M}_5$ (9)	Hot Spots (10)
Ia	0755E	25–end	16.0–27.0	1.7–2.4	flat	−	0.80	1.2	
	1357S	12–end	10.0–15.2	1.3–1.6	steep	−	0.94	1.4	
	1357N	5–8	4.2–6.7	1.0–1.5	steep	+	1.00	1.9	
	1357N	13–end	10.8–15.8	1.8–2.6	flat	0	1.00	1.9	
	1450W	5–end	7.5–15.3	1.4–1.7	flat	+	1.17	1.9H	
	1638W	4–6.5	6.4–10.2	1.2–1.5	steep	−	1.04	1.9	
	1658W	12–18	5.9–8.8	1.7–2.6	steep	−	1.56	1.4	
	1827E	12–end	10.4–22.0	1.1–1.5	flat	0	0.78	0.9	
	1827W	5–22	4.3–19.1	1.0–2.1	flat	−	1.11	1.7	
Ib	0034E	2–6	0.9–2.7	0.70–1.1	flat	0	1.41	1.7	
	1357S	3–8	2.5–6.7	0.61–1.1	steep	+	0.94	1.4	
	1450E	2–5	2.2–7.5	0.71–1.1	flat	0	1.10	1.1	
II	0206W	4–8	2.1–4.2	0.09–0.13	steep	+	0.16	2.0	
	0836N	10–25	10.2–25.4	0.11–0.12	steep	+	0.09	1.3H	
	1113W	10–end	6.7–15.1	0.11–0.15	flat	−	0.09	3.6H	**
	1243S	20–end	22.5–52.9	0.41–0.42	steep	+	0.22	3.3H	
	1243N	10–30	11.3–33.8	0.03–0.03	flat	+	0.02	1.8H	*
	1521S	10–18	10.6–19.0	0.08–0.10	steep	+	0.02	2.4H	**
	1553W	12–end	7.1–15.8	0.49–0.69	steep	+	0.39	1.6	
	1658W	2–4	0.7–2.0	0.42–0.96	steep	+	1.56	1.4	
	1752E	5–9	3.1–5.5	0.26–0.32	steep	+	0.29	3.9H	
	2116S	2–7	0.5–1.7	0.57–0.79	flat	0	1.61	0.6	

X-ray data is $\bar{\beta}_X = 0.68 \pm 0.09$; that is, very similar to the mean β derived from the radio data. (The Thomas et al. values of β were corrected by the well-known factor of 3/2 necessitated by their use of the Jones and Forman 1984 model; see Killeen and Bicknell 1988.)

b) The Jet Parameters: η and $\mathcal{M}$

The basic density ratio parameter $\eta_0 = \rho_{\text{jet},0}/\rho_{\text{ext},0}$ refers to an arbitrarily chosen starting point of the integration, which is usually located around $4''$–$5''$ from the core. However, the starting point has no physical significance, because it is located at an arbitrary linear distance from the nucleus. Therefore, we introduce other reference points; first, the density ratio at the beginning of the collimation plateau, η_p, and second, the density ratio at a fixed linear distance of 5 kpc from the core, η_5 (see Table 4). In the following, we mainly use η_5, since it is available for all jets (contrary to η_p); moreover, η_5 and η_p are well correlated. In Figure 5, we show the histogram of η_5 values determined from the model fitting. The median value of η_5 is close to unity; that is, the jet and external densities are very similar at a distance of 5 kpc from the core. Only in a few objects do we find jets with $\eta_5 < 0.1$. Therefore, the jets in low-luminosity galaxies have generally reached density equilibrium by about 5 kpc from the core. Nevertheless, it should be noted that most of the starting values of η for these jets are less than unity. The jets which have $\eta_0 \sim 1$ are in the higher redshift galaxies of our sample (except B2 1553 + 24), so that we are only starting to resolve the jets near 5 kpc. The derived Mach numbers (again referred to the fixed reference point at 5 kpc) are sometimes rather uncertain, but in most cases we know that the best fit at least lies in the interval $1 < \mathcal{M} < 3$. In roughly one-third of the jets, the χ^2 distribution as a function of $\mathcal{M}$ is very shallow, such that values of $\mathcal{M}$ up to ~ 10 can still give good fits (not more than 1 σ away from the χ^2_{min} fit; we indicate such objects with an H in column [9] of Table 4, and we refer to them loosely as "high-$\mathcal{M}$ jets" hereafter). At first

sight, this is disappointing, because it means that $\mathcal{M}$ is not well constrained, but we show in the next section that, on the contrary, some interesting conclusions can be drawn for these sources. We note here that almost all of these high–Mach number jets are of low density (i.e., $\eta_5 < 0.3$), except one, viz. the west jet of B2 1450 + 28. In this particular case, which we also discussed above, the best fit gives a very small core radius, especially when compared to the core radius derived from the eastern jet. Considering this and the fact that the fit is of rather low quality, the solution may very well be wrong.

c) Quality of the Fits

In § IVd, we use the parameters derived from the model fits (i.e., η, $\mathcal{M}$, β, and r_c), as well as the mean spreading rate $d\Phi/d\Theta$ of the jets and the total and jet radio power at 20 cm; the latter data were taken from Paper VI. Before doing that, we first discuss the quality of the model fits.

In column (5) of Table 1, we have given a very general classification of the jets in terms of S (smooth), B (blobby), and SB (partially blobby). Hereafter, the SB jets are lumped together with the B type. Since the B jets show, by definition, brightness enhancements, which may be indicative of physical processes that are not incorporated in the model (dissipation, shocks, etc.), we expect a priori the fits to be less satisfactory for such jets than for the smooth jets. Inspection of the χ^2_{red} values in Table 2 confirms this; the smooth jets have a median $\chi^2_{\text{red}} = 2.97$, against $\chi^2_{\text{red}} = 6.20$ for the blobby jets. A more subjective judgement, based on eye inspection of Figures 2 and 4, agrees very well with the χ^2_{red} values given in Table 2. Moreover, there is a clear difference in the kind of solution we find; 10 of the 11 smooth jets have a sharp χ^2_{min} at low values of the Mach number. On the other hand, six out of seven of the high–Mach number jets (i.e., those objects for which high values of $\mathcal{M}$ are allowed) are blobby. This probably points to a real physical difference; it is reasonable that jets with Mach numbers higher than about 2 or 3 would produce strong internal shocks which

would account for strong surface brightness enhancements along their lengths.

It is worth noting that three of the four jets with $\beta = 0.4$ are classified B. This fairly low value of β may reflect the lack of inclusion of dissipation in the model; in order to compensate for lack of dissipation, a fully adiabatic jet model requires more deceleration, which in turn requires a flatter pressure gradient.

d) General Correlations

In general, there are no strong correlations, either among the model parameters or between the model parameters and spreading rate and radio power. However, there are some interesting tendencies, based upon our breakdown of the sample into low–Mach number jets and high–Mach number jets, which are worth noting.

1. *Light jets have a higher Mach number.*—In Figure 6, we have plotted $\mathcal{M}_{5\,kpc}$ against $\eta_{5\,kpc}$. Note that the crosses represent *high–Mach number* jets, i.e., jets with a large permissible range of $\mathcal{M}$ according to the definition given above, as opposed to the *low–Mach number* jets, which definitely have $\mathcal{M} \sim 2$. Taking all points together, there does not appear to be any correlation between η_5 and $\mathcal{M}_5$, but once we note that the crosses represent jets that allow much higher Mach numbers almost equally well, the picture changes drastically. All jets with low Mach numbers (the open circles in Fig. 6) have $\eta_5 > 0.1$, whereas four out of seven high–Mach number jets have $\eta_5 < 0.1$. In fact, the low-$\mathcal{M}$ jets have a median $\eta_5 = 1.00 \pm 0.14$, against $\eta_5 = 0.09 \pm 0.08$ for the high-$\mathcal{M}$ jets. The difference is clearly seen in the histogram in Figure 7.

2. *Low-density, high–Mach number jets occur in sources with higher radio power.*—In Figure 8, the total radio power–density ratio diagram is shown. As before, only a weak correlation is apparent, but 6/7 of the high–Mach number jets are at high radio luminosities ($P > 10^{24}$ W Hz^{-1}). The median total radio powers are $\log P_{tot} = 24.03 \pm 0.15$ for low-$\mathcal{M}$ jets, and $\log P_{tot} = 24.41 \pm 0.06$ for the high-$\mathcal{M}$ jets. Thus, the jets in our high–Mach number category are very close to the critical power for transition to Fanaroff-Riley class II. This is consistent (see B86a) with the notion that the Fanaroff-Riley classification is strongly related to the jet Mach number. A similar
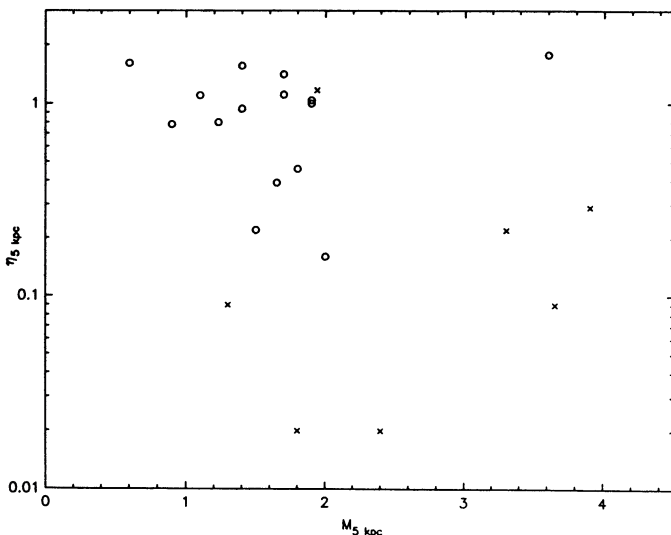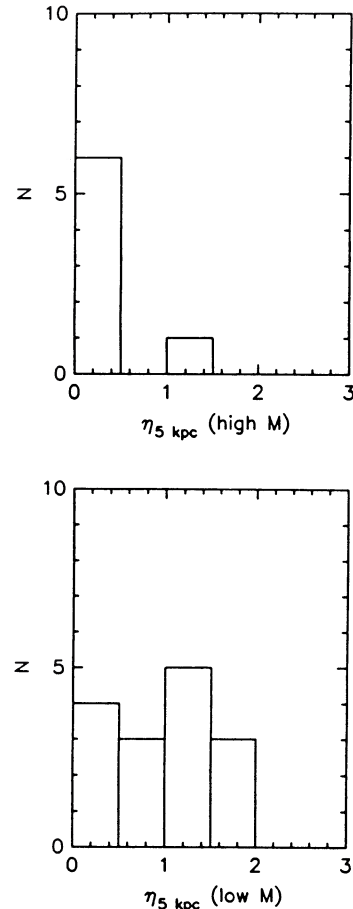

FIG. 7.—Histograms of η_5 for high-$\mathcal{M}$ (*upper*) and low-$\mathcal{M}$ (*lower*) jets.

effect is found if we use the jet radio power (see Paper VI) instead of the total power.

3. *High–Mach number, low-density jets are more collimated.*—This is perhaps the clearest trend of all: the high–Mach number jets are predominantly located in the

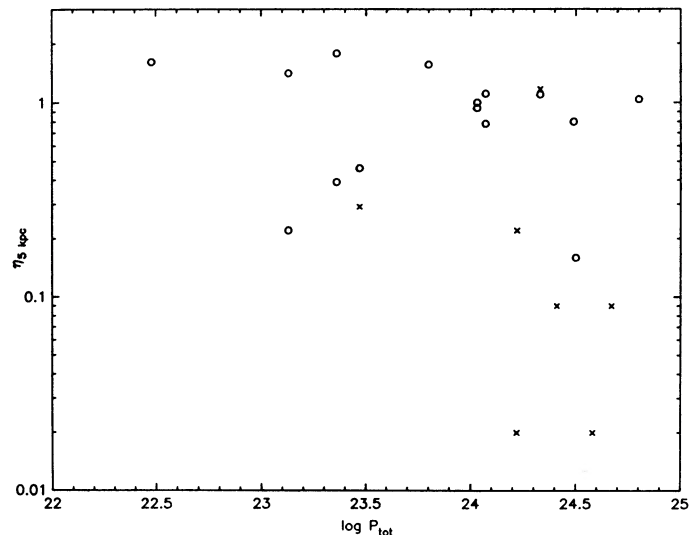FIG. 6.—η_5 against $\mathcal{M}_5$. Crosses are the "high"-$\mathcal{M}$ jets (see text).

FIG. 8.—η_5 against the logarithm of the total source power (in W Hz) at 1.4 GHz. The meaning of the crosses is the same as in Fig. 6.
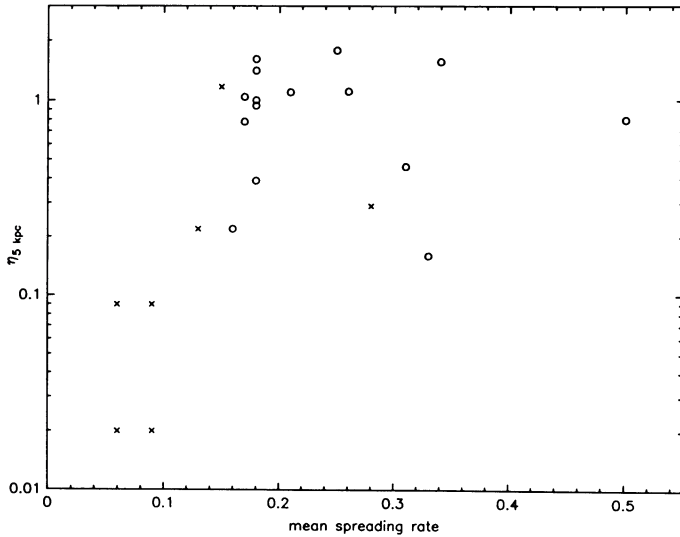
FIG. 9.—η_5 against the jet's main spreading rate. The meaning of the crosses is the same as in Fig. 6.

region of small η_5 and small average $d\Phi/d\Theta$ (see Fig. 9). Note also that the only high-density, high–Mach number jet (B2 1450 + 28W) has a relatively small spreading rate, which reinforces our suspicion that we have arrived at a wrong solution in this particular case. The low-$\mathcal{M}$ objects have a median $d\Phi/d\Theta = 0.18 \pm 0.03$, the high-$\mathcal{M}$ jets have a median $d\Phi/d\Theta = 0.09 \pm 0.02$. This is consistent with the lower spreading rate of high–Mach number jets and the consequent lower rate of entrainment.

No other correlations have been found. At most, we could say that there is a slight tendency for light, high–Mach number jets to occur in galaxy atmospheres with a small core radius.

e) Correlations Between the Two Sides of a Radio Source

Of the 23 jets given in Table 1, 16 form pairs. Leaving out B2 0206 + 35 (the eastern jet does not have sufficient data to constrain the fit), we have seven sources with two-sided jets. The model parameters of both sides are compared in Figure 10. The galactic atmosphere parameters agree well, except for two sources. One discrepant source is B2 1752 + 32, where on one side our model solution requires $\beta = 0.7$ and on the other side $\beta = 0.4$. A second, obvious discrepancy is the difference in core radius between the two sides of B2 1450 + 28: the model solutions give 3 and 0.2 kpc, respectively. We have already mentioned this source as being anomalous, and this is probably one case where we did not arrive at a satisfactory solution. In all other cases, β and r_c are either very similar or identical on both sides of the source.

f) The Collimation Plateau and the Jet Velocities

Of the 23 jets in the sample, 19 have a well-defined collimation plateau (and some even two), where the value of $d\Phi/d\Theta$ is close to zero. Our most favored explanation for this phenomenon is that the jet does not sustain the level of turbulence that it initially has close to the core (this turbulence is probably generated by disruptive shocks and maintained by shear), and this leads to a reduction in the spreading rate. This effect will be enhanced if the jet is still light at this stage, so that the positive buoyancy force can accelerate it. If buoyancy is implicated, then the jet should still be light at the beginning and
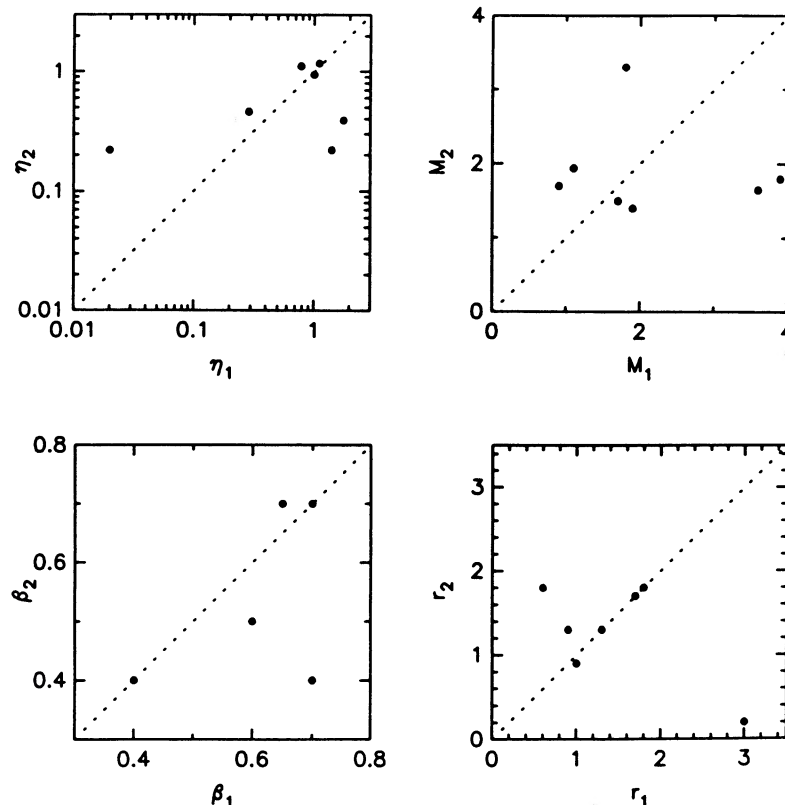
FIG. 10.—The model parameter on one side of a source (subscript 1) against the corresponding parameter on the other side (subscript 2)

over much of the collimation plateau. However, the lightness of the jet is not strictly necessary. If $\bar{\eta}_p \sim 1$ (where $\bar{\eta}_p$ is the mean density ratio in the collimation plateau), there will be no, or hardly any, positive buoyancy force, so that the velocity and density of the jet in a well-collimated region will remain constant. The density *ratio* η will then increase, since the external density always decreases. This increase will be even more pronounced if $\bar{\eta}_p > 1$, because then the negative buoyancy will brake the jet, which will cause compression and hence an increasing jet density.

Since three of the 19 jets mentioned above have two collimation plateaus, we have a total number of 22 collimation plateaus, given in Table 4, where we list the location of the plateau (cols. [3] and [4]), the initial and final density ratio (col. [5]), the pressure and velocity gradients (cols. [6] and [7]), the density ratio and Mach number at 5 kpc from the radio core (cols. [8] and [9]) and the presence of hot spots at the end of the jet (col. 10: an asterisk indicates a brightness enhancement, two asterisks indicate a true hot spot). We have grouped together the jets that are heavy in the collimation plateau ($\bar{\eta}_p \geq 1$: group I) and the ones that are light ($\bar{\eta}_p < 1$: group II). A further distinction can be made between jets that have $\eta_p > 1$ everywhere in the plateau (group Ia) and the jets with $\eta < 1$ at the beginning of the plateau (group Ib).

As can be seen from Table 4, the jets in general behave as expected: a heavy jet enters a collimation zone when $\mathcal{M}$ increases, but its velocity is constant or decreases. In this region, we always have $d\eta/d\Theta > 0$, although this increase is not due to entrainment. There are two exceptions: both B2 1357 + 28N and B2 1450 + 28W have $dv/d\Theta > 0$. We note, however, that their brightness fits, described in the previous sections, are rather poor. We can therefore safely discard these two fits. The three jets in group Ib have a nondecreasing velocity in the collimation zone, and this is also expected: for these objects, the buoyancy force should be close to zero, at least on average, such that $v \sim$ constant and $d\eta/d\Theta > 0$ due to the decrease of the external density. It is also readily understood why the collimation zones with $\eta \sim 1$ are typically found at the end of the jets: since the jets are decelerated, they cannot progress much further. At most, the radio emitting material may form disconnected clumps or filaments after the ending of the jet, which may still move outward at low velocities.

Ten of the collimation zones in Table 4 are of the second type ($\eta < 1$). The fit duly produces the acceleration caused by the buoyancy force ($dv/d\Theta > 0$), while the density ratio is approximately constant. Thus, the density of the jet actually decreases in the collimation plateau, if the jet is light. There is one object that does not behave correctly: in the collimation region of B2 1113 + 29, the velocity is decreasing. Note also that in this case, the brightness fit is not very satisfactory, especially in the collimation plateau itself.

It is worth noting that none of the objects in group I have hot spots at the end of the jets, against two (B2 1113 + 29 and B2 1521 + 28) in group II. One more jet (B2 1243 + 26N) ends in a bright, extended blob. These two, or three, jets are among the lightest in the sample ($\eta \leq 0.1$): such light jets (with possibly supersonic velocities even at their end points) are exactly the ones that are expected to show hot spots, due to the sudden compression where the jet impinges upon an intergalactic medium, which is denser than the jet.

So far, we have discussed velocity gradients, not the absolute values of the velocity. However, it is possible to give two independent estimates of the jet velocity, for example at the fiducial point Θ_0. The first comes from the parameters determined in the model fitting. Since we assume pressure equilibrium between the jet and the external medium and since we determined the density ratio and the Mach number, for a rough estimate of the jet velocity it is sufficient to know the temperature of the galactic atmosphere, which can be obtained from β and the stellar velocity dispersion (see § IV*h*). Not surprisingly, the jets with $\eta_0 \geq 0.1$ all have velocities around 1000 km s^{-1} (a factor of order $\mathcal{M}$ greater than the stellar velocity dispersion). It is only for light jets that the velocity estimates go up to 10^4 km s^{-1} (B2 1521 + 28). An independent velocity estimate can be obtained from the energy budget discussed in B86*a*. The values obtained for the three sources for which spectral index information is available are listed in Table 6. The estimated velocities are again of order a few thousand km s^{-1}. We come back to the velocity estimates in § IV*i*.

g) The Lobe Pressure

The asterisks in Figure 2 indicate the average equipartition pressures of the lobes (if any lobe is present). In some sources, the lobe pressure is about an order of magnitude below the extrapolated pressure of the King model of the galactic atmosphere that was used in the jet-fitting procedure. The sources with a lobe pressure at least 5 times below the King model pressure are: B2 0836 + 29 ($\sim$10), B2 1113 + 29 ($\sim$8), B2 1243 + 26 north ($\sim$9) and south ($\sim$5), B2 1450 + 28 west ($\sim$6) and B2 1638 + 32 ($\sim$5). It is striking that four of these five radio galaxies are located in rich (Abell) clusters, while the environment of the fifth (B2 1638 + 32) is not known, but it is a highly distorted source (see the radio image in Paper I). The effect is illustrated in Figure 11; there is a significant difference between the pressure ratios $P_{\text{King}}/P_{\text{Lobe}}$ of sources inside and outside rich clusters. In fact, since pressure ratios ≤ 3 cannot be considered to be significantly different from unity, in view of the uncertainties involved, all sources that are located outside a rich cluster show good agreement between the extrapolated King model pressure and the lobe equipartition pressure. Note
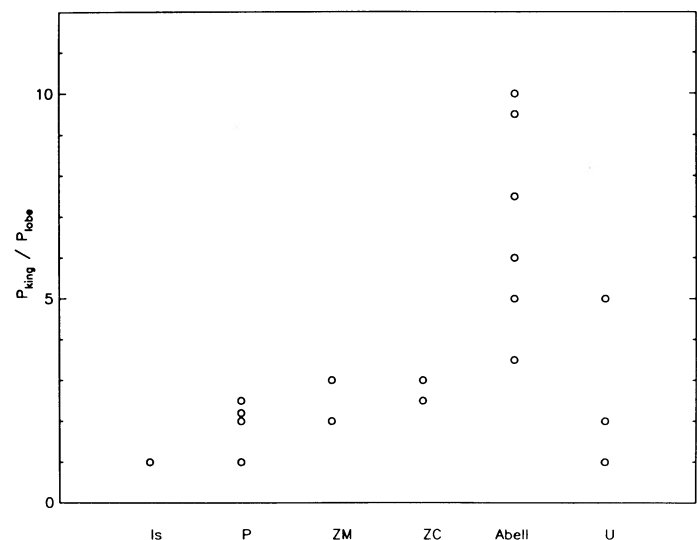

Fig. 11.—The ratio of the extrapolated pressure of the King atmosphere and the minimum pressure in the lobe, for different types of galactic environments: Isolated (Is) galaxies, galaxies in poor clusters (P), in medium compact (ZM) and compact (ZC) Zwicky clusters, and in Abell clusters. For a few radio galaxies, the type of environment is unknown (U).

that the agreement becomes even better if the pressure of sources outside rich clusters flattens less quickly toward the background value (see Fig. 2).

There are several possible explanations for the correlation displayed in Figure 11. First, King's model applies to the potential of an isolated galaxy. In reality, the potential is the sum of that due to the galaxy and the cluster, so that the atmospheric pressure decreases further with distance from the center of the cluster rather than remaining constant, as implied by the King model. This decrease is more marked in clusters with deeper potential wells; that is, in richer clusters. Second, the equipartition pressure may be well below the atmospheric pressure, if a substantial fraction of the lobe pressure is provided by thermal material that has been mixed with the nonthermal plasma. It may well be that such mixing is particularly important in rich clusters, because of the high density of the intergalactic medium. The third possibility is related to the second: the higher density in rich clusters may cause fragmentation of the radio emitting material in which case the lower pressure is simply due to a small filling factor, not taken into account in the minimum pressure calculation. The fourth possibility is that the pressure of the galactic atmosphere at large distances from the center of the galaxy is lower than expected, owing to ram pressure stripping. This may be an attractive hypothesis, because the sources with high pressure discrepancies, which are located in rich clusters, all have very distorted lobes or are of the wide-angle–tail (WAT) type (like B2 0836 + 29, B2 1450 + 28, and B2 1638 + 32). The radio galaxies are probably moving with respect to the cluster gas, and this may lead to stripping of the galactic atmosphere. The King pressure profile of the galaxy should therefore have a cutoff, beyond which the pressure drops abruptly to the level of the intergalactic medium. This effect is not unlikely, since some of the sources are rather large (~ 300 kpc, both B2 0836 + 29 and B2 1243 + 26).

There are some X-ray data (Morganti *et al.* 1987) for B2 0836 + 29 and B2 1113 + 29 which shed some light on the above possibilities. For the former source, Morganti *et al.* found that the ratio of the pressure of the X-ray–emitting gas to the lobe minimum energy pressure, $P_{th}/P_{nth} \approx 4.4$, indicating mixture of thermal and nonthermal gas in the lobe. At the position of the lobe, the thermal pressure is a factor of 0.4 below the central cluster pressure, and it is the latter pressure that corresponds to the background pressure of the King model. That is, the central cluster pressure gives the background value for the atmosphere of the galaxy. Taking these two numerical factors into account implies a ratio $P_{nth}/P_{King} \approx 0.1$, which is what is observed. Thus, in this case, it appears that a combination of distance from the center of the cluster and mixing of thermal and nonthermal material can explain the ratio of lobe pressure to background King pressure.

The same cannot be said for B2 1113 + 29, whose western lobe (the one in question) is close enough to the center of the cluster that the decreasing pressure of the cluster atmosphere is unimportant. (See Morganti *et al.* 1987 for a map of the radio source overlain on the X-ray map.) Moreover, $P_{th}/P_{nth} \approx 0.7$, so that there is no case for the mixing of thermal and nonthermal gas. However, unlike B2 0836 + 29, the center of this galaxy is not situated precisely at the cluster center, raising the possibility that it is moving significantly with respect to the intergalactic medium and that ram pressure stripping is important.

h) The M/L Ratios

We can use the King galactic atmospheres of § III to estimate the masses of the radio galaxies. The mass of a King model,

$$M(r) = \frac{3\sigma^2 r_c}{G} K\left(\frac{r}{r_c}\right) = 6.25 \times 10^{10}\left(\frac{\sigma}{300 \text{ km s}^{-1}}\right)^2$$
$$\times \left(\frac{r_c}{\text{kpc}}\right) K\left(\frac{r}{r_c}\right) M_\odot, \quad (4.1)$$

where σ is the central line-of-sight velocity dispersion and $K(r/r_c)$ is a function which is related to the particular King model. Blue luminosities were determined from the absolute visual magnitudes given in Table 1, assuming $B - V = 1.0$. We calculated M/L_B for the region of the galaxy corresponding to the optical extent as measured from the Palomar sky survey plates; that is, in calculating $K(r/r_c)$ and $M(r)$ we used $r(\mu_B = 25.0$ mag arcsec$^{-2})$. We estimated velocity dispersions from the Faber-Jackson (1976) relation ($L \propto \sigma^4$) and the blue magnitudes in Table 1 and took $\sigma = 210$ km s^{-1} for an absolute magnitude $M_B = -18.5$ (note that we adopt a Hubble parameter of 100). The resulting values are given in Table 5, which also contains the optical radii in kiloparsecs and the velocity dispersions, σ_{FJ}, estimated from the Faber-Jackson relation. Note that we use the projected core radius, $r_{c,p}$ estimated from the model fits in calculating the mass. This should introduce no systematic errors, since as we noted in § III, it is likely that most jets are nearly at right angles to the line of sight.

The values of M/L in Table 5 do not exhibit any systematic dependence on redshift indicating that our model fits are consistent. Nevertheless, the mean $\langle M/L \rangle = 24 \pm 5$ is somewhat larger than the mean value of approximately 14 that is usually found for elliptical galaxies (see Smith and Bicknell 1986; Efstathiou, Ellis, and Carter 1980). This difference is large enough to be interesting, but better estimates of galaxy luminosities and velocity dispersions are required before our estimated M/L values can be relied upon. Of course, the difference could be due to a radially increasing M/L. We also note that Heckman (1983) has claimed that radio loud galaxies have a larger M/L than radio quiet ellipticals with $\Delta(M/L_B) \sim 5$–10. If this is true, our higher mean M/L may reflect this. Planned CCD observations and optical velocity dispersion measurements will address these questions.

TABLE 5

M/L VALUES

B2 Name	$r(\mu_B = 25.0)$ (kpc)	L_B ($10^{10} L_\odot$)	σ_{FJ} (km s^{-1})	M/L
0034 + 25	13	2.04	320	30
0206 + 35	16	3.24	360	27
0755 + 35	17	3.24	360	11
0836 + 29	22	5.62	410	20
1113 + 29	16	3.24	360	22
1243 + 26	19	3.24	360	31
1357 + 27	18	3.55	360	26
1450 + 28	15	2.69	340	22
1521 + 28	16	2.59	350	31
1553 + 24	13	1.86	310	26
1638 + 32	24	6.76	430	20
1658 + 30	10	1.07	270	22
1752 + 32	15	2.69	340	25
1827 + 32	18	3.55	360	25
2116 + 26	12	1.70	300	28

i) *Jet Velocities and the Energy Budget*

The velocities of the jets may be estimated directly from the best-fit parameters using

$$v_{jet} = \mathcal{M}\left(\frac{4P}{3\eta\rho_{ext}}\right)^{1/2} = \mathcal{M}\left(\frac{4kT}{3\mu m_p\eta}\right)^{1/2} = \mathcal{M}\left(\frac{4\sigma^2}{3\eta\beta}\right)^{1/2} , \quad (4.2)$$

where the expressions given in § III relating the parameter β to the atmospheric temperature, T, and the line-of-sight velocity dispersion, σ, have been used. The velocities calculated in this way for both the initial integration points and points 5 kpc from the core are given in Table 6. We have also calculated κ, the ratio of the luminosity of each lobe to an estimate of the energy flux (at 5 kpc) of the jet feeding it. The energy flux was calculated using equation (7.2) of B86*b*, namely,

$$F_E = 1.5 \times 10^{40}\left(\frac{\sigma}{300 \text{ km s}^{-1}}\right)\left(\frac{\Phi}{kpc}\right)^2 P_{-11}\beta^{-1/2}\eta^{-1/2}$$

$$\times \mathcal{M}\left(1 + \frac{\mathcal{M}^2}{6}\right) \text{ergs s}^{-1} , \quad (4.3)$$

using the parameters estimated from the model fits and the minimum pressure.

The estimates of jet energy flux, lobe luminosity, and κ are also given in Table 6 for those sources in which there is an obvious lobe. In two sources (B2 0206 + 35 and B2 1113 + 29), spectral index measurements are available which indicate a steepening of the spectrum and for these independent estimates (κ_{est}; see Table 6) can be made using the theory for the energy budget developed in B86*a*. In these two sources, the values of κ are in good agreement.

The parameter κ can approach unity for lobes in which the age of the source is greater than radiative time scale of the lobe, $t_{rad} = E_{lobe}/\mathscr{L}_{lobe}$, where E_{lobe} and $\mathscr{L}_{lobe}$ are the lobe energy and luminosity, respectively. For half the jets, the values of κ are on the order of 0.1, as argued in B86*a*. However, there are a

number of jets for which κ is greater than 0.4, including four jets for which $\kappa \gtrsim 0.8$. This may indicate that the lobes of these sources are approaching radiative equilibrium with the jet energy flux, or that the jet parameters (in particular η and $\mathcal{M}$) are poorly estimated. It is impossible to make a judgement on this until further jet models are developed which take dissipation into account. Moreover, when estimating κ, factors of order unity can be important. For example, the lobe luminosities have been calculated using a cutoff frequency of 10^{10} Hz. If the cutoff is 10^9 Hz, the lobe luminosity is reduced by a factor of 0.6. Furthermore, the jet energy flux may be underestimated by a factor of a few owing to our use of the minimum pressure. Nevertheless, the fact that κ only exceeds unity in one problem source (B2 1450 + 28; see § IV*a* above) is a reasonable indication of the consistency of the model.

If the values of κ in some sources are too high (and our limited experience in estimating this parameter seems to indicate that values $\kappa \sim 0.1$ may be appealing), then the jet velocity estimates for such sources are too low. As a glance at Table 6 shows, all the high-κ sources have estimated jet velocities below 1000 km s^{-1}, so that adjusting the velocities of these jets by an order of magnitude has no effect on the conclusion that class I jet velocities are generally below 10,000 km s^{-1}. (For low Mach numbers, the jet energy flux is proportional to the velocity.) On the other hand, a low-velocity jet would take longer to build up an observable flux of radio emission, so that it is entirely consistent that low-velocity jets are found in sources that are older in comparison to the radiative time scale. Moreover, it is reasonable to suppose that higher velocity sources contain a higher magnetic field, making the observation of spectral steepening more likely. Indeed, the sources for which we do have spectral index information have minimum energy lobe magnetic fields, which are a factor of 2 higher than the average of the other sources in the sample. At the same time, sources with higher velocity jets are preferentially observed at an earlier time in their evolution, making it

TABLE 6
Jet Velocities

B2 Name	v_0 (10^3 km s^{-1})	v_5 (10^3 km s^{-1})	F_E (10^{41} ergs s^{-1})	$\mathscr{L}_{lobe}$ (10^{41} ergs s^{-1})	κ	κ_{est}
0034 + 25E	0.94	0.62	0.22	0.085	0.4	...
0034 + 25W	1.4	1.4	0.33	0.060	0.2	...
0206 + 35E	2.8	2.0	14	1.2	0.1	0.2
0206 + 35W	5.9	2.5	7.4	1.2	0.2	0.2
0755 + 35E	0.62	0.49	1.9	1.7	0.9	...
0836 + 29N	3.2	2.7	5.2	1.4	0.3	...
1113 + 29W	10	7.8	15	2.0	0.1	0.1
1243 + 26N	9.1	8.2	7.9	0.7	0.1	...
1243 + 26S	3.6	4.5	12	2.1	0.2	...
1357 + 27N	0.75	0.95	0.9	0.6	0.7	...
1357 + 27S	0.56	0.72	0.6	0.5	0.8	...
1450 + 28E	0.46	0.49	0.8	1.6	2.0	...
1450 + 28W	0.93	0.83	1.5	0.9	0.6	...
1521 + 28S	12	6.8	8.4	3.2	0.4	...
1553 + 24E	1.3	1.2	4.2	...	...	...
1553 + 24W	2.3	1.1	2.2	...	...	...
1638 + 32W	1.3	1.2	9.8	6.0	0.6	...
1658 + 30W	0.68	0.35	0.3	0.2	0.7	...
1752 + 32E	3.1	3.4	2.5	...	...	...
1752 + 32W	4.9	1.6	2.0	...	...	...
1827 + 32E	0.85	0.55	0.7	0.5	0.7	...
1827 + 32W	0.94	0.95	1.2	0.9	0.8	...
2116 + 26S	0.63	0.18	0.068	...	...	...

more likely that they would be observed with a lower value of κ. Thus, our prejudice toward $\kappa \sim 0.1$ may well be based upon observational selection effects.

V. CONCLUSIONS

We have shown that, with some qualifications, jets in low-luminosity radio galaxies can be described successfully by the model presented in B86b. The qualifications principally relate to the neglect of dissipation and the fits are better for smoother jets which show no evidence of dissipation through shocks or turbulence. It is possible for the jets classified as B or SB that the model underestimates the value of the atmosphere parameter β, so that more rapid deceleration can compensate for dissipation. However, the good statistical agreement between our estimates of β and independent X-ray estimates of this parameter for other ellipticals shows that the adiabatic assumption in the model is reasonable. We have also examined the results of our model fitting for consistency from several points of view. For example, we have successfully examined the internal consistency of the models in the various collimation plateaus. The general success of the model in producing consistent results means that the physical picture of class I jets as turbulent, decelerating, low-velocity flows is basically correct.

The weaker jets in our sample appear to be heavier on average (with a density ratio typically ~ 0.5) than the more powerful ($P \geq 10^{24.0}$ W Hz^{-1}) jets. Moreover, they have $M \sim 2$, whereas the stronger may have $M > 3$. We have analyzed this in more detail by investigating the behavior of the jet parameters (density ratio, velocity, and Mach number) in the collimation plateaus, i.e., in regions where the jet recollimates after a phase of expansion. The impression is that there are two distinct groups of radio jets in our sample, with one group representing the truly low luminosity (or class I) sources, while in the other group the jets have properties which begin to resemble those of powerful class II sources. It is probably no coincidence that at the lowest luminosities where hot spots are found, low-density, high–Mach number jets are beginning to occur that are also well collimated.

Since relatively heavy jets quickly reach, partly by entrainment and partly because the galactic atmosphere becomes more tenuous, a density contrast of order unity with respect to the external medium, they cannot grow much larger than the dimensions of the parent galaxy. This is an attractive explanation for the small (~ 10–20 kpc) size of many weak radio sources.

An inevitable conclusion from this paper is that the velocities of class I jets are low. A direct calculation, based on the estimated jet parameters, gives velocities of the order of 1000–10,000 km s^{-1}. Again, the jets identified as light with high Mach number are at the higher end of this range. Consideration of the energy budget in these sources shows consistency (for all but one source) with the notion that the ratio, κ, of lobe luminosity to jet energy flux should be less than unity. However, there are a number of sources for which this ratio approaches 1. This could indicate that these sources are approaching radiative equilibrium, that we have underestimated the jet energy flux by using the minimum pressure, or that some jet parameters (principally the density ratio, η, and the Mach number, $\mathcal{M}$) are poorly estimated. Nevertheless all these "high κ" jets have estimated velocities less than 1000 km s^{-1}, and reducing κ by an order of magnitude will not increase their velocities beyond 10,000 km s^{-1}.

We have approximated the galactic atmospheres by King models and have found plausible values for the two characteristic parameters, the core radius, r_c, and the ratio of virial temperature to gas temperature, β. The distribution of β has been discussed above. The core radii (of order 1–2 kpc) are more typical of cD galaxies than of giant ellipticals. This is not surprising, since many of the B2 galaxies are known to be cD's, but we refer again to the comments on the core radius made in § III.

Using the King models, we have given an estimate of the mass to luminosity ratio out to the $\mu_B = 25.0$ mag arcsec^{-2} isophote. There is no dependence of M/L on L, but the mean value ($M/L = 24$) is higher than is normally found for giant ellipticals ($M/L = 14$). Considering the uncertainties in the determination of M/L, we consider the difference not to be significant at this stage. Nevertheless, even for an M/L of 24, no large missing mass out to ~ 10–20 kpc is required to explain the dynamics of radio jets in low luminosity radio galaxies.

REFERENCES

Bicknell, G. V. 1984, Ap. J., 286, 68 (B84).
———. 1986a, Ap. J., 300, 591 (B86a).
———. 1986b, Ap. J., 305, 109 (B86b).
Bridle, A. H. 1984, A.J., 89, 979.
de Ruiter, H. R., Parma, P., Fanti, C., and Fanti, R. 1986, Astr. Ap. Suppl., 65, 111 (Paper II).
Efstathiou. G., Ellis, R. S., and Carter, D. 1980, M.N.R.A.S., 193, 931.
Faber, S. M., and Jackson, R. E. 1976, Ap. J., 204, 668.
Fanaroff, B. L., and Riley, J. M. 1974, M.N.R.A.S., 167, 31P.
Fanti, C., Fanti, R., de Ruiter, H. R., and Parma, P. 1986, Astr. Ap. Suppl., 65, 145 (Paper III).
———. 1987, Astr. Ap. Suppl., 69, 57 (Paper IV).
Fanti, R., Lari, C., Parma, P., Bridle, A. H., Ekers, R. D., and Fomalont, E. B. 1982, Astr. Ap., 110, 169.
Heckman, T. M. 1983, Ap. J., 273, 505.

Hoessel, J. G. 1980, Ap. J., 241, 493.
Jones, C., and Forman, W. 1984, Ap. J., 276, 38.
Killeen, N. E. B., and Bicknell, G. V. 1988, Ap. J., 325, 165.
Morganti, R., Fanti, C., Fanti, R., Parma, P., and de Ruiter, H. R. 1987, Astr. Ap., 183, 203 (Paper V).
Norman, M. L., Winkler, K.-H. A., and Smarr, L. L. 1984, in Physics of Energy Transport in Extragalactic Radio Sources, ed. A. H. Bridle and J. A. Eilek (Green Bank: NRAO), p. 150.
Parma, P., de Ruiter, H. R., Fanti, C., and Fanti, R. 1986, Astr. Ap. Suppl., 64, 135 (Paper I).
Parma, P., Fanti, C., Fanti, R., Morganti, R., and de Ruiter, H. R. 1987, Astr. Ap., 181, 244 (Paper VI).
Smith, R. M., and Bicknell, G. V. 1986, Ap. J., 308, 36.
Thomas, P. A., Fabian, A. C., Arnaud, K. A., Forman, W., and Jones, C. 1986, M.N.R.A.S., 222, 655.

G. V. BICKNELL: Mount Stromlo and Siding Spring Observatories, Private Bag, Woden P.O., A.C.T. 2606, Australia

H. R. DE RUITER, R. FANTI, R. MORGANTI, and P. PARMA: Istituto di Radioastronomia, Via Irnerio, 46, 40126 Bologna, Italy